River Flow 2010 - Dittrich, Koll, Aberle & Geisenhainer (eds) - © 2010 Bundesanstalt für Wasserbau ISBN 978-3-939230-00-7

Numerical simulation of ripple formation

Yan Cui
Graduate School of Science & Engineering, Ritsumeikan University, Kusatsu, Japan

Y Q. Nguyen
Dept. of Fluid Mechanics, Ho Chi Minh City University of Technology, Ho Chi Minh City, Vietnam

John C. Wells
Dept. of Science & Engineering, Ritsumeikan University, Kusatsu, Japan

ABSTRACT: Based on Large Eddy Simulation (LES) in a doubly periodic domain, two of us (Nguyen and Wells 2009) have developed a model to simulate the initial formation of sedimentary bedforms, constrained to be two-dimensional, in hydraulically smooth turbulent flows under bedload conditions. The LES is coupled with an Immersed-Boundary Method (IBM) to efficiently handle the evolving bed geometry without re-gridding. Given the instantaneous bed geometry, the LES yields a bed shear stress distribution. At each flow cross-section, the spanwise average of this bed stress was taken to determine the sediment flux according to the van Rijn (1984) formula chosen for its applicability to particle Reynolds numbers in the hydraulically smooth regime. In the present contribution, we extend the above model to simulate the formation of three-dimensional bedforms. Simulated results for initial ripple development change very little from the 2D bed model. Three-dimensional "bumps" can be observed on the bed surface. With small "bumps" on the bed surface the three-dimensional bed model slightly speeds the process of erosion of the downstream end, and shortens the time to form a new sand wave, and shortens the length of the first wave. Flows over fixed beds with two-dimensional and three-dimensional "bumps" suggest that non-uniformity of shear stress in the spanwise direction can reduce the mean shear stress and sediment flux of the ripples.

Keywords: *Sediment transport, Bedforms, Turbulent flows, Large-Eddy-Simulation, Ripples*

1 INTRODUCTION

When a riverbed or seabed is eroded by a current, the bed usually becomes unstable and bedform patterns appear. In this paper our attention is mainly focused on subaqueous sedimentary ripples, which are small-scale patterns characterized by a height of the order of a centimeter that are observed to appear only in hydro-dynamically smooth and transitional flows, i.e. for the grain Reynolds number $\mathrm{Re}_p \le 24.0$ (Sumer and Bakioglu, 1984). There are important motivations for researchers to study the appearance and the time development of the ripples:

- The presence of ripples may change the bed roughness, which determine the fluid shear stress near the bed;
- Ripples usually cause the separation of the bottom boundary layer and strongly modify the sediment transport;

There are a few theoretical works describing sand wave development from a flat bed: Kennedy (1963) is considered to be the first one who laid the foundation of the descriptions of the geometry of the sand waves on streambeds (Raudkivi 1997). The model is based on a two-dimensional inviscid potential flow over an erodible bed. He related the local sediment transport rate to the local fluid velocity, with a lag distance between the two, which is the key factor for producing unstable waves. Later, Richards (1980) added viscous effects to the flow model with an one-dimensional turbulence model for flows with hydro-dynamically rough beds to study the formations of ripples and dunes. His results showed that formation of ripples is independent of the flow depth. This work was extended to the region of hydro-dynamically smooth flows by Sumer & Bakioglu (1984) for analyzing ripple formations. This analysis predicted that ripples would exist only when grain Reynolds number $\mathrm{Re}_p \le 24.0$.

Several researchers have applied numerical methods to simulate the flows over fixed ripples to understand the effects of bedform to the flow fields and the implications for sediment transport. For example, Zedler and Street (2001) focused on

the initial entrainment and transport of suspended sediment in flows over fixed ripples. A well-resolved large-eddy simulation (LES) was employed to examine in some detail the role and effect of coherent structures that occur near the bed.

However, to the authors' knowledge, there have been no reported simulations of the formation process of ripples from an initially flat bed by a well-resolved turbulent flow field.

Numerical models for simulating bedload transport must include a model to solve the flow field and thence the stress distribution on the bed surface, a model to transport the sediment along the bed, and a model to describe the evolution of the bed elevation according to the transport of the sediment(Kennedy 1963, Richards 1980, Sumer and Bakioglu 1984, Bui et al. 2004). Among available methods which explicitly represent the turbulent flow fields, DNS (Direct Numerical Simulation), LES and RANS (Reynolds-Averaged Navier-Stokes equations) can be considered. DNS is far too costly, leaving LES and RANS as feasible candidates (Keylock et al. 2005, Giri and Shimizu 2006) at present. Keylock et al (2005) suggested that LES is preferable for fluvial geomorphic and sedimentological research, since most RANS models are intended for accurate representations of the mean flow field only. Chang & Scotti (2003) compared LES with a RANS k-ω model for separating flows over ripples, and reported that RANS substantially under-predicted Reynolds stress and over-predicted vertical velocity, while LES agreed very well with DNS and experiment.

A two-dimensional numerical model has been developed in our lab to study the detailed information of ripple initiation and evolution under an uniform turbulent current (Nguyen and Wells 2009). Bedload sediment flux is estimated by the van Rijn's (1984) formula from the time-averaged bed shear stress distribution obtained from flow solutions by a Large-Eddy-Simulation (LES) method coupled with an Immersed-Boundary-Method (IBM). Evolution of the bed surface, as described by the Exner equation, is computed quasi-simultaneously with the flow field.

However, when bedforms are three-dimensional, as often found for ripples formed in alluvial channels, the sediment transport is not uniform in the spanwise direction, therefore three-dimensional bedload models are necessary.

In the two-dimensional model by Nguyen and Wells (2008), Re_p was varied in the range [0.5, 2.5]. The wavelengths of the earliest ripples obtained at each Re_p are plotted in Figure 1, together with the experimental results by Kuru et al. (1995), Coleman and Melville (1996), Coleman et al. (2003), and Langlois and Valance (2007). The computed points are distributing on the lower limit of the experimental ones shows the agreement between them.

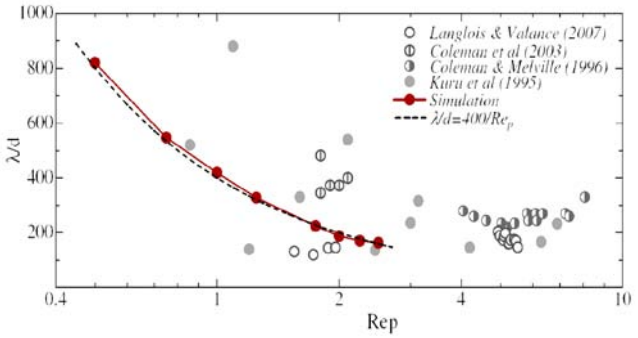

Figure 1. Length of the first sand wave developing from a flat bed: numerical (Nguyen and Wells 2008) vs. experimental results.

As the first step to developing a three-dimensional model of ripple formation, this paper applies the local shear stress instead of the transversely-averaged bed shear stress to compute bedload flux. Similar to the two-dimensional model, we simulated the formation process of the first ripple under hydraulically smooth conditions, namely with a grain Reynolds number Re_P of 0.5. Results of the 2D and 3D models are compared. We found that smaller-scale "microforms" appear on the bed surface in the three-dimensional model, and to distinguish these from the main ripple initiated in both models, we refer to these smaller structures as "bumps" in this paper. To understand their effect, the distribution of bedload transport capacity around fixed "bumps" is discussed.

2 NUMERICAL MODEL

To build a computational model to study the initiation and evolution of ripples, simplifying assumptions are unavoidable. The present work assumes that

- The flow is hydrodynamically smooth (the grain Reynolds number $\mathrm{Re}_p \le 2.5$), i.e. roughness of the bed is neglected (Yalin 1977);
- Suspended sediment may be neglected, i.e. only bedload transport is observed to dominate ripple formation(Mantz 1992, Coleman and Melville 1996, Coleman et al. 2003, Langlois and Valance 2007);
- Time scale of flow development is much shorter than that of the bedform development (Richards 1980). Accordingly, the bed surface is treated as fixed while the flow field is solved in an interval of 100 time steps to allow the flow field to adapt to the new bed profile.

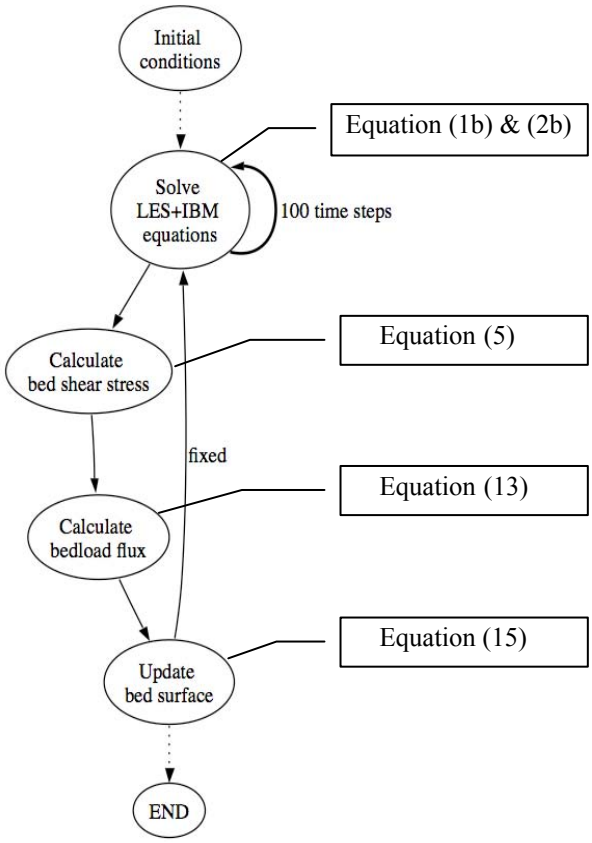

Figure 2. Computational procedure.

Figure 2 shows the main computational procedure of the model. First the initial bed profile, flow conditions (domain size, grid generation, Reynolds number) and sediment conditions are specified. Our model uses a rectangular domain and a Cartesian grid. The three-dimensional flow fields are solved by an LES method coupled with IBM while the bed surface is fixed. After solving this hydrodynamic model over 100 time steps, the time averaged flow fields are applied to compute the bed shear stress. Then the bedload flux is estimated by the van Rijn's formula (1984), and the bed surface is updated by the Exner equation. These three steps are iterated continuously.

2.1 *The Governing Equations of Flow*

The governing equations for LES coupled with IBM are the incompressible N-S equations, as filtered by a low-pass spatial filter. In IBM an artificial body force f is added to impose the no-slip condition at solid boundaries:

$$\frac{\partial \overline{u}_j}{\partial x_j} = 0 \tag{1a}$$

$$\frac{\partial \overline{u}_i}{\partial t} + \overline{u}_j \frac{\partial \overline{u}_i}{\partial x_j} = -\frac{1}{\rho}\frac{\partial \overline{p}}{\partial x_j} - \frac{\partial \tau_{ij}}{\partial x_j} + \nu \frac{\partial^2 \overline{u}_i}{\partial x_j \partial x_j} + f_i \tag{2a}$$

where "¯" indicates the filter operator, $\overline{u}_i$ is the filtered velocity component in the i direction, i = 1, 2, 3, and $(x_1, x_2, x_3) = (x, y, z)$, ρ is the fluid density, p is the dynamic pressure, τ_{ij} is the subgrid stress(SGS), and ν is the fluid kinematic viscosity.

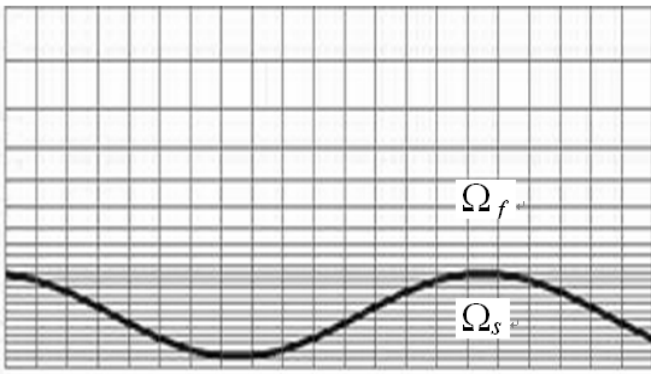

Figure 3. An example of IBM grid for computing flows over a wavy bed.

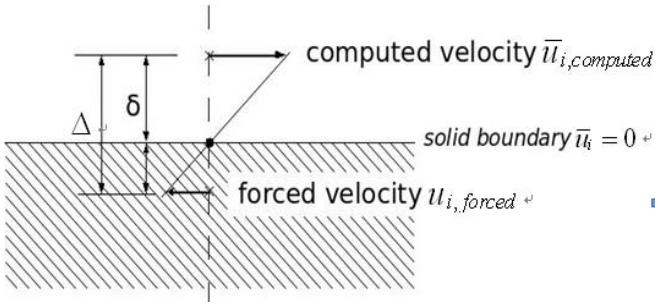

Figure 4. Forcing strategy in IBM.

The subgrid stress model is the Shear-Improved Smagorinsky model proposed by Lévêque et al. (2007):

$$\tau_{ij} - \frac{1}{3}\delta_{ij}\tau_{kk} = -2\nu_T \overline{S}_{ij} \tag{3}$$

with $\overline{S}_{ij} = \frac{1}{2}\left(\frac{\partial \overline{u}_i}{\partial x_j} + \frac{\partial \overline{u}_j}{\partial x_i}\right)$,

$\nu_T = \left(C_s\overline{\Delta}\right)^2\left(\left|\overline{S}\right| - \left|\left\langle \overline{S} \right\rangle\right|\right)$, and $\left|\overline{S}\right| = \left(2\overline{S}_{ij}\overline{S}_{ij}\right)^{1/2}$,

where C_s=0.16 and $\overline{\Delta} = \left(\overline{\Delta}_x\overline{\Delta}_y\overline{\Delta}_z\right)^{1/3}$.

$\overline{\Delta}_x$, $\overline{\Delta}_y$ and $\overline{\Delta}_z$ are the local grid spacings in the x, y and z-directions, respectively. < > denotes "local ensemble average", which is performed in the spanwise direction for models of two-dimensional bedload, and in both spanwise direction and along time in models of three-dimensional bedload.

In IBM, the computational domain includes both the solid portions, Ω_s, and the fluid portions, Ω_f, on a fixed Cartesian grid system, and the same governing equations are applied on the whole domain; see Figure 3. The artificial body force f is added to the Navier-Stokes equation to account for the presence of the solid portions. IBM simplifies grid generation, and avoids regenerating the computational grid as the solid domain changes shape.

The artificial force f is used to represent the solid parts, so f is nonzero only on the solid portion, i.e. $f_i = 0$ in Ω_f

There are many strategies for the artificial body force f. Fadlun et al. (2000) proposed a linear *velocity interpolation* method. The velocity of the point nearest to the solid surface is computed via a linear interpolation so that it satisfies $\overline{u}_i = 0$ right on the solid boundary (fixed bed). As shown in Figure 4, let Δ and δ be the grid spacing and the distance from the point outside but nearest to the solid surface, respectively; $\overline{u}_{i,computed}$ be the velocity obtained from equation (1a) and (2a) at the point outside, but nearest to the solid surface; and $u_{i,forced}$ is the imposed velocity at the point inside but nearest to the solid surface. According to Fadlun et al. (2000), $u_{i,forced}$ can be computed as follows:

$$u_{i,forced} = -\overline{u}_{i,computed}\frac{\Delta - \delta}{\delta} \tag{4}$$

The governing equation (1a) and (2a) are nondimensionalized by the fluid density ρ, mean friction velocity $u_{\tau 0}$ and total flow depth H. Each variable in equation (1a) and (2a) is nondimensionalized as followings:

$$\tilde{t} = \frac{t}{H/u_{\tau 0}},\ \tilde{x}_i = \frac{x_i}{H},\ \tilde{\tau}_{ij} = \frac{\tau_{ij}}{u_{\tau 0}^2}, \tilde{P} = \frac{p}{\rho u_{\tau 0}^2} + \tilde{\tau}_{kk},$$
$$\tilde{f}_i = \frac{f_i H}{u_{\tau 0}},\ Re_\tau = \frac{u_\tau H}{\nu}.$$

where "~" indicates a nondimensionalized parameter. The governing equations become:

$$\frac{\partial \tilde{\overline{u}}_j}{\partial \tilde{x}_j} = 0 \tag{1b}$$

$$\frac{\partial \tilde{\overline{u}}_i}{\partial \tilde{t}} + \tilde{\overline{u}}_j \frac{\partial \tilde{\overline{u}}_i}{\partial \tilde{x}_j} = -\frac{\partial \tilde{P}}{\partial \tilde{x}_j} + (\tilde{\nu}_T + \frac{1}{Re_\tau})\frac{\partial^2 \tilde{\overline{u}}_i}{\partial \tilde{x}_j \partial \tilde{x}_j} + \tilde{f}_i \tag{2b}$$

These equations are solved by a finite difference method on a fixed Cartesian, staggered nonbodyfitted grid with 4th-order central discretization in space and 2nd-order Adams-Bashforth method for time marching (e.g., Geurts 2003).

2.2 *Boundary Conditions*

Periodic boundary conditions are applied in the stream (x) and span (z) directions. No-slip conditions are applied at the lower boundary and free-slip conditions on upper boundary.

The artificial force f by IBM can be replaced by an implicit boundary condition: The velocities at points inside Ω_s are set to zero, but at points nearest to the bed surface they are computed by equation (4).

2.3 *Sediment Motion*

In the present model, the shear velocity u_τ is computed from the shear stress, as averaged during an interval of 100 LES time steps:

$$u_\tau^2 = \nu \frac{\partial \overline{u}_\varsigma}{\partial \eta_\varsigma} \tag{5}$$

where $\overline{u}_\varsigma$ is the time-averaged velocity component along the bed surface, and η is the surface-normal direction. In our model, we use two definitions of $\overline{u}_\varsigma$: transversely averaged velocity in two-dimensional bed model and local velocity in three-dimensional bed model.

Neglecting effects of relative density, local bedload flux is normally assumed to depend on two nondimensional parameters, the grain Reynolds number:

$$\mathrm{Re}_p = \frac{u_{\tau 0} d}{\nu} \tag{6}$$

and the local Shields number θ is:

$$\theta = \frac{u_\tau^2}{(s-1)gd} = \left(\frac{u_\tau}{u_{\tau 0}}\right)^2 \theta_0 \tag{7}$$

where θ_0 is the mean Shields number:

$$\theta_0 = \frac{u_{\tau 0}^2}{(s-1)gd} \tag{8}$$

s is the ratio of grain density to fluid density, d is the grain diameter.

There are a number of formulae for bedload transport proposed in the literature (Cheng 2002). Most of them are valid only for high grain Reynolds numbers. To our knowledge, the only formula that is also valid for low grain Reynolds numbers is the equilibrium bedload flux equation by van Rijn (1984):

$$q_{eq} = 0.053 \frac{T^{2.1}}{d_*^{0.3}} \left[(s-1)g\right]^{1/2} d^{1.5} \tag{9}$$

where $\tilde{q}_{eq}$ is the equilibrium bedload flux, and d_* is the particle mobility parameter:

$$d_* = \left[\frac{1}{\theta_0}\mathrm{Re}_p^2\right]^{1/3} \tag{10}$$

and T is the transport stage parameter

$$T = \frac{\theta}{\theta_c} - 1.0 \tag{11}$$

in which θ_c is the critical Shields parameter which is modeled as a formula of Re_p. Kovacs and Parker (1994) proposed a vectorial formulation for θ_c on combined transverse and longitudinal sloping beds:

$$\left|\frac{\theta_c}{\theta_{c0}}\hat{s}+\frac{\bar{k}_t}{\tan\varphi_s}\right|=\left|\bar{k}_n\right| \tag{12}$$

where θ_{c0} is the critical Shields number for zero-slope bed, $\hat{s}$ is the direction of shear stress, $\bar{k}_n$ (respectively, $\bar{k}_t$) is the component of the unit vertical vector normal (tangent) to the tangent plane to the bed surface. The friction angle φ_s is reported in the range of $\tan\varphi_s$ =[0.35-0.72] with an average of $\tan\varphi_s$ =0.63(Richards 1980).

According to Kennedy (1963) and Nakagawa & Tsujimoto (1980), one of the principal causes of bed instability is a phase lag between the sediment transport and the bed shear stress. To model this lag, or the non-equilibrium nature of sediment transport, "the rate of sediment exchange between bed and flow was assumed proportional to the difference between the actual instantaneous sediment load and the equilibrium sediment load, and related to the so called non-equilibrium adaptation length, which characterizes the distance for sediment to adjust from a non-equilibrium state to an equilibrium state" (Phillips and Sutherland 1989). Quantifying this concept, Bui et al. (2004) proposed a non-equilibrium bed-load transport equation:

$$\frac{\partial\left(\alpha\tilde{q}_b\right)}{\partial x}+\frac{\partial\left(\beta\tilde{q}_b\right)}{\partial z}=-\frac{\tilde{q}_b-\tilde{q}_{eq}}{\tilde{l}_{eq}} \tag{13}$$

where $\tilde{q}_b$ is the local bedload transport rate, x is the longitudinal direction, z is the transverse direction, α, β are the direction cosines determining the components of $\tilde{q}_b$, i.e. the direction cosines of $\hat{s}$ in x and z directions, determined by equation (12); α =1, β =0 in our two-dimensional bedload model. $\tilde{l}_{eq}$ is the bedload adaption length. Significant dependence of results on the adaptation length parameter has been reported (Armanini and Di Silvio 1988, Thuc 1991, Wu et al. 2004); here we adopt the adaption length taken as the average saltation step length proposed by van Rijn, (1984):

$$\tilde{l}_{eq}=3\left(\frac{d}{H}\right)d_*^{0.6}T^{0.9} \tag{14}$$

Evolution of the bed surface is described by the Exner equation

$$\left(1-n\right)\frac{\partial\tilde{h}}{\partial\tilde{t}}=-\left(\frac{\partial\left(\alpha\tilde{q}_b\right)}{\partial x}+\frac{\partial\left(\beta\tilde{q}_b\right)}{\partial z}\right) \tag{15}$$

where $\tilde{h}$ is the evolution of the bed surface and n is the porosity of the bed material.

More details and validations of the two-dimensional model can been found in (Nguyen and Wells 2008).

3 NUMERICAL RESULTS AND DISCUSSION

Figure 5 shows a simulation of the evolution from an initial bed profile with one sinusoidal half-wave by the two-dimensional bedload model (Nguyen and Wells 2008), and Figure 6 shows corresponding results from the current three-dimensional bedload model, for H^+ = 300, Re_p=0.5 and θ_0 = 0.55 , The grid is (256 × 72 × 32) points in a domain of ($H_x = 7.68H$) × ($H_y = H$) × ($H_z = 0.96H$) with $\Delta_x^+ = \Delta_z^+ \approx 30.0$, and $\Delta_{y\,\min}^+ = 0.93$. The depth of sand is $0.05H$ and the height of the initial sand wave is $A = 0.002H$. The bed profile is plotted at different nondimensionalized time, $\tilde{t} = tu_{\tau 0}/H$.

Again, both models employ a fully 3D turbulent flow solver; the difference is that the 3D model uses the local shear stress, instead of the shear stress averaged in the z direction over the entire width, to estimate the fluxes of the bedload transport. In both cases, the crest of the initial wave first grows in height. The wave crest then broadens streamwise until the downstream end of the wave starts being eroded strongly, with the scoured sediment deposited further downstream. Once two troughs fore and aft of the wave can be identified, the wave is identified as "sand-wavelet".

As seen in Figure 6, the 3D bed model predicts small "bumps" (much smaller than the new ripple) on the bed surfaces because of the unevenly distributed local shear stress. These "bumps" propagate along the flow direction and have little effect on the shape of the initial sand wave. At the time $\tilde{t}$ =6.2, the downstream end began to erode strongly in the three-dimensional model, while, similar erosion did not start in the two-dimensional model until $\tilde{t}$ =7.3. It appears that the application of local shear stress shortens the time when erosion of the downstream end begins, and leads to a decrease of the length of the first wave.

Figure 7 compares the bedforms from the two-dimensional and three-dimensional models results when $\tilde{t}$ =6.2 (the time when the first sand waves appeared in the three-dimensional model as in Figure 6) and also shows two-dimensional model when $\tilde{t}$ =7.3 (the time when the first sand waves appears by two-dimensional model as in Figure 5). The results of three-dimensional models are averaged in the z direction. From these figures, the

most important conclusion is that the results change rather little when a 3D bed model is employed. We can see that the three-dimensional model results in a slightly slower propagation of the sand wave.

Figure 8 shows the mean streamwise velocity of the flow fields near the bed surface(y/H=0.05). U_b presents the bulk velocity and <U> is the mean streamwise velocity averaged in the x-z plane and over time from $\tilde{t}=100$ to $\tilde{t}=200,000$. The mean velocity in the three-dimensional model is a little smaller than in the two-dimensional model.

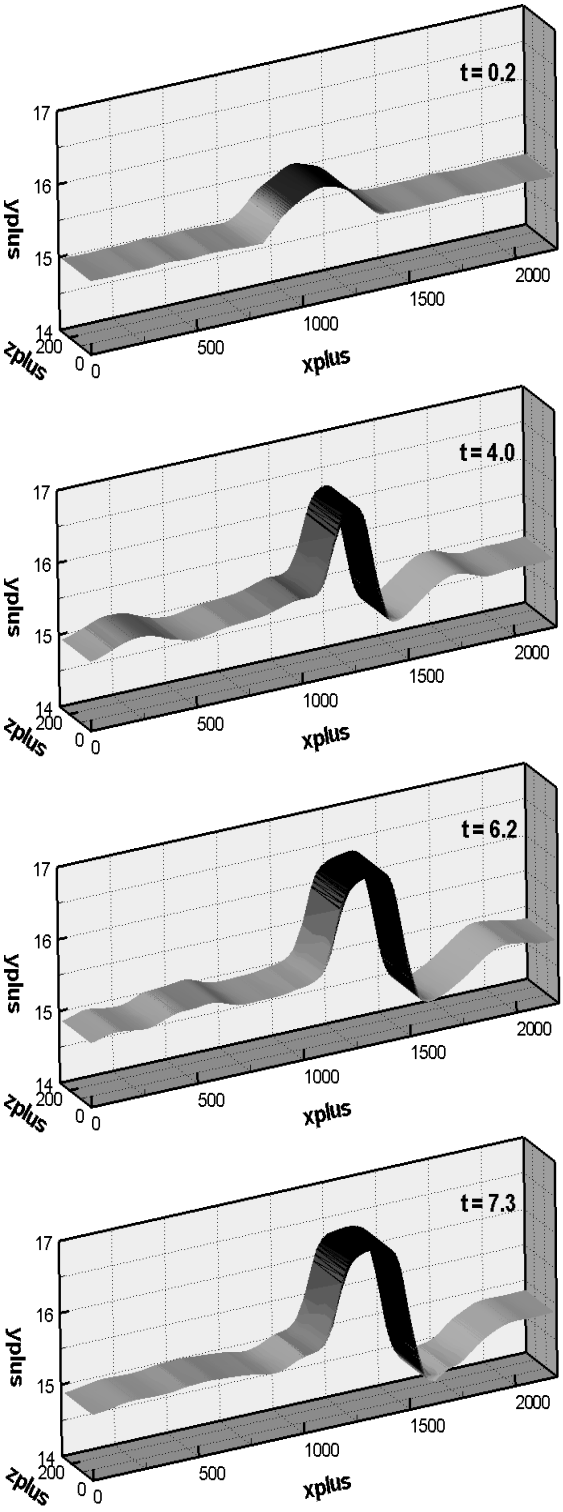

Figure 5. Sand wave developing by two-dimensional bed-load model (From top: $\tilde{t}$ =0.2, 4.0, 6.2, 7.3)

As the velocity near the bed is quite slow, the difference reaches about 10% at some points near the bed. This shows that the existence of "bumps" in the 3D model has little effect on the whole flow field, but may have a significant effect on the near-bed flow field.

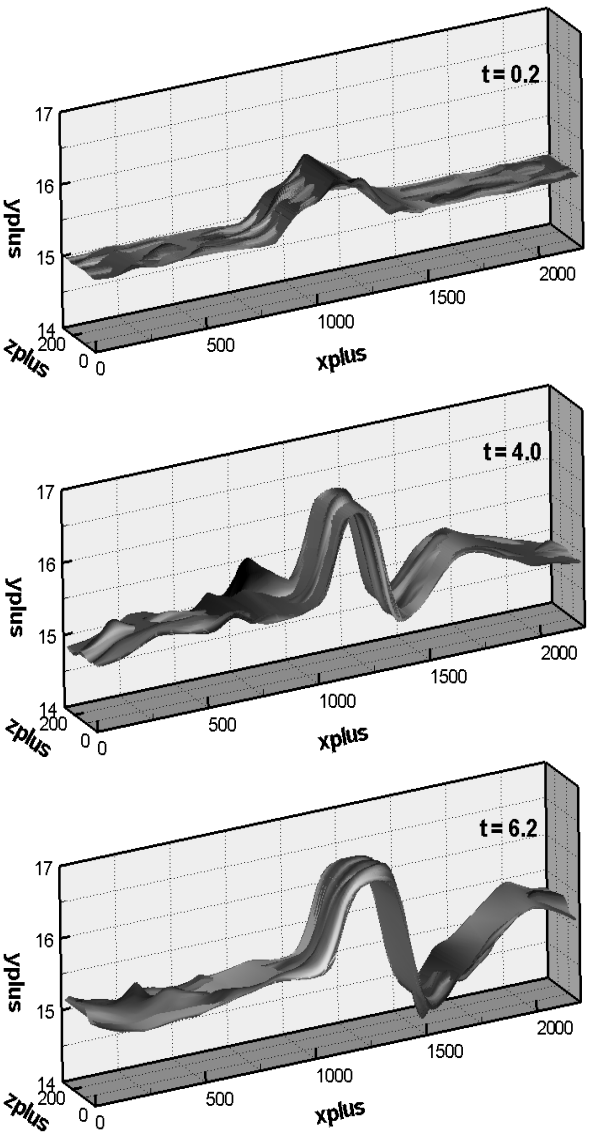

Figure 6. Sand wave developing by three-dimensional bed-load model (From top: $\tilde{t}$ =0.2, 4.0, 6.2)

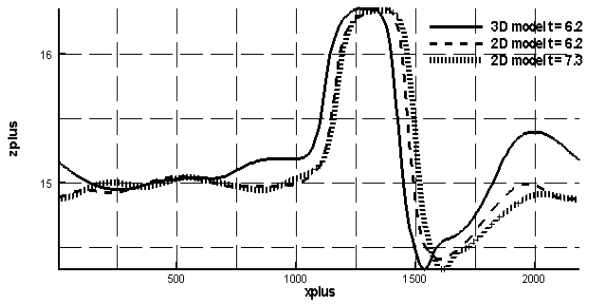

Figure 7. Comparison of results from three-dimensional model (average in z direction) with two-dimensional model when $\tilde{t}$ =6.2 and $\tilde{t}$ =7.3

In results from the three-dimensional bed model (Figure 6), the largest height of the small "bumps" Y^+ is about 1.0. To understand the effects of such a bump on the bed shear stress distribu-

tion, flows over 2D and 3D "bumps" on a flat bed with heights Y^+=1.0, shown in Figure 9, were simulated. Shear stress and potential sediment flux averaged in the z direction are compared in Figure 10. The peaks of the friction velocity distributions always occur upstream of the peak of the "bumps", i.e. there is a phase lag between the two. The lag $\tilde{l}_{eq}$ between the shear stress and the sediment flux of equation (13) is not visible in this figure as the saltation step length is around 5 crested-ripples. This helps to explain the somewhat slower propagation of the sand wave in the 3D model. Nguyen (2008) concluded that the sandwave is affected by the strong gradient of the bed shear stress around the downstream area. The existence of the small "bumps" reduces the shear stress gradient, thus the sand wave moves slower. However, the existence of the small "bumps" may increases the sediment flux around a small area, which may explain why the three-dimensional model shortens the time when erosion of the downstream end begins (Figure 7).

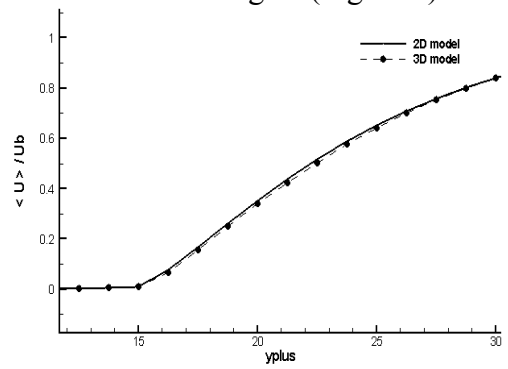

Figure 8. Comparison of the mean quantity of flow fields near the bed surface(y/H=0.05). U_b presents the bulk velocity and <U> is the mean streamwise velocity averaged in x-z plane and over time

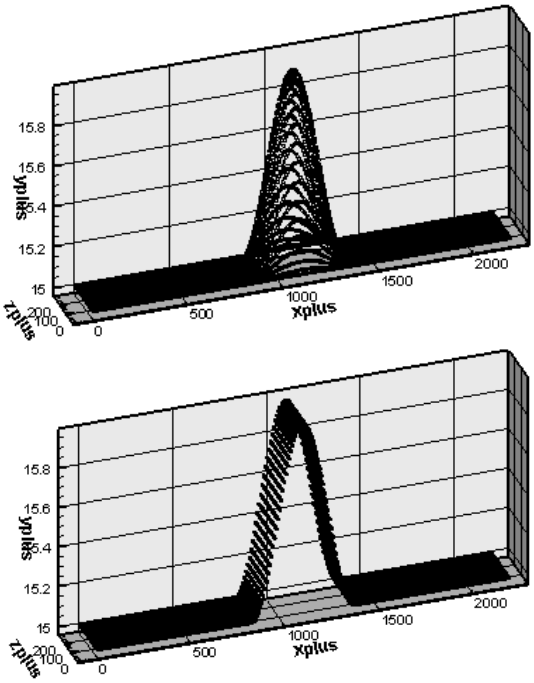

Figure 9. Forms of small "bumps" over flat beds (Top: 3D bump; Bottom: 2D bump) used in fixed-bed tests

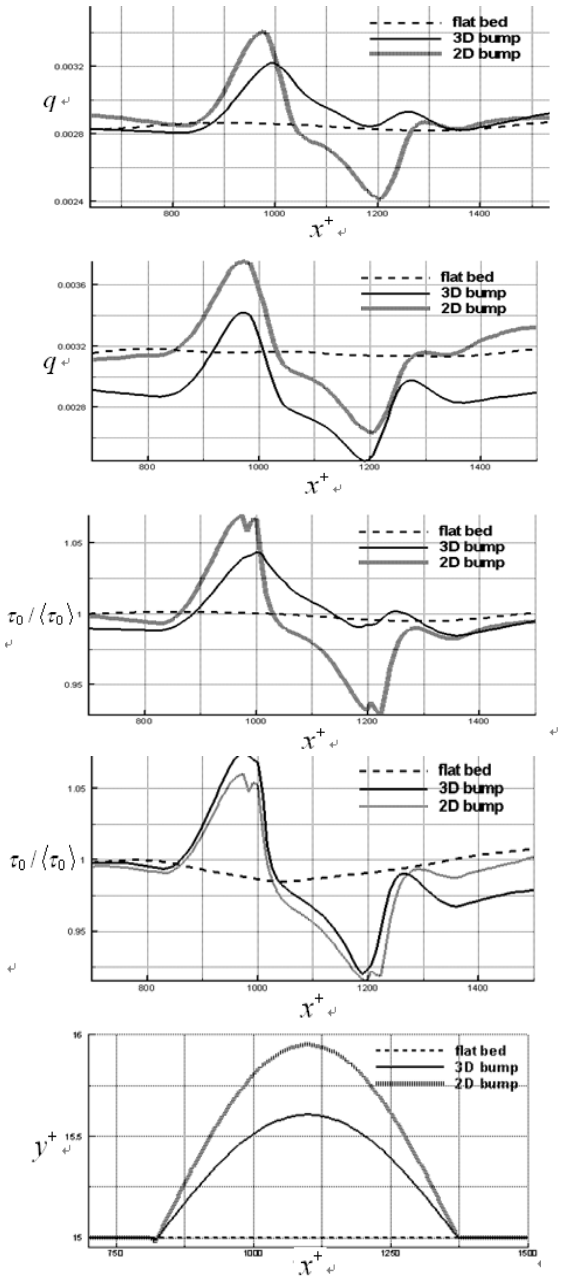

Figure 10. Comparison of mean characters over fixed small "bumps" on a flat bed (averaged in z direction: a) sediment flux $\tilde{q}_b$ averaged in the span direction; b) sediment flux $\tilde{q}_b$ averaged in the central x-y plane ($z = nz / 2$); c) bed shear stress $\tau_0 / <\tau_0>$ averaged in the whole domain; d) bed shear stress $\tau_0 / <\tau_0>$ averaged in the central x-y plane ($z = nz / 2$); e) bed level Y^+).

4 SUMMARY & CONCLUSION

A three-dimensional bedload model has been applied in our computer code for simulating the initial evolution of ripples. Thanks to the detailed flow field information computed by the LES-IBM model, the local shear stress is available to estimate the fluxes of three-dimensional bedload transport. The comparison to the 2D span-averaged shear stress model is discussed. Overall results for initial ripple development change very little from the 2D bed model. With small "bumps" on the bed surface, the three-dimensional model slightly speeds the process of erosion at the down-

stream end, and shortens the time to form a new sand wave and the length of the first wave.

Flows over fixed beds with two-dimensional and three-dimensional "bumps" help to understand the effect of the shear stress non-uniformity in the spanwise direction. We concluded that this uniformity can reduce the mean shear stress and sediment flux of the ripples.

Up to the present, our 3D bed model has just been tested with a representative value grain Reynolds number Re_p=0.5. As shown in Figure 1, Re_p=0.5 is near the smallest experiment value in available literature. That figure shows that wavelengths predicted by the 2D bed model are, in fact, independent of particle diameter. Thus raising Rep to more common values did not change the wavelength, and we hypothesize that it would not affect other characteristics of early-stage ripples. However, more tests with Re_p varying in the range [0.5, 2.5] are needed to confirm or reject this hypothesis. Beyond that, it is important to extend the LES-IBM technique to handle transitional roughness, i.e. $Re_p > 2.5$.

REFERENCES

Armanini, A., and G. Di Silvio. 1988. One-Dimensional Model for the Transport of a Sediment Mixture in Non-Equilibrium Conditions. Journal of Hydraulic Research JHYRAF. 26(3).

Bui, Minh Duc, T. Wenka, and W. Rodi. 2004. Numerical Modeling of Bed Deformation in Laboratory Channels. J. Hydr. Engrg. 130(9): 894-904.

Chang, Yeon S., and Scotti, Alberto. 2003. Entrainment and Suspension of Sediments into a Turbulent Flow over Ripples. Journal of Turbulence. 4(1): 019.

Cheng, N. 2002. Exponential Formula for Bedload Transport. J. Hydr. Engrg. 128(10): 942-946.

Coleman, S.E., J.J. Fedele, and M.H. Garcia. 2003. Closed-Conduit Bed-Form Initiation and Development. J. Hydr. Engrg. 129(12): 956-965.

Coleman, S.E., and B.W. Melville. 1996. Initiation of Bed Forms on a Flat Sand Bed. J. Hydr. Engrg. 122(6): 301-310.

Fadlun, E.A., R. Verzicco, P. Orlandi, and J. Mohd-Yusof. 2000. Combined Immersed-Boundary Finite-Difference Methods for Three-Dimensional Complex Flow Simulations. J. Comput. Phys. 161(1): 35-60.

Geurts, B. 2003. Elements of Direct and Large-Eddy Simulation. RT Edwards.

Giri, S., and Y. Shimizu. 2006. Numerical Computation of Sand Dune Migration with Free Surface Flow. Water Resources Research. 42(10): 10422.

Kennedy, J.F. 1963. The Mechanics of Dunes and Antidunes in Erodible-Bed Channels. Journal of Fluid Mechanics. 16: 521–544.

Keylock, C., R. Hardy, D. Parsons, R. Ferguson, S. Lane, and K. Richards. 2005. The Theoretical Foundations and Potential for Large-Eddy Simulation (LES) in Fluvial Geomorphic and Sedimentological Research. Earth-Science Reviews. 71(3-4): 271-304.

Kovacs , A., and G. Parker. 1994. A New Vectorial Bedload Formulation and its Application to the Time Evolution of Straight River Channels. Journal of Fluid Mechanics. 267: 153–183.

Kuru, W.C., D.T. Leighton, and M.J. McCready. 1995. Formation of Waves on a Horizontal Erodible Bed of Particles. International Journal of Multiphase Flow. 21(6): 1123–1140.

Langlois, V., and A. Valance. 2007. Initiation and Evolution of Current Ripples on a Flat Sand Bed under Turbulent Water Flow. The European Physical Journal E: Soft Matter and Biological Physics. 22(3): 201–208.

Lévêque, E., F. Toschi, L. Shao, and J.P. Bertoglio. 2007. Shear-Improved Smagorinsky Model for Large-Eddy Simulation of Wall-Bounded Turbulent Flows. Journal of Fluid Mechanics. 570: 491–502.

Mantz, P.A. 1992. Cohesionless Fine-Sediment Bed Forms in Shallow Flows. Journal of Hydraulic Engineering. 118(5): 743–764.

Nakagawa, H., and T. Tsujimoto. 1980. Sand Bed Instability due to Bed Load Motion. J. Hydraul. Div. 106: 2029–2051.

Nguyen Quoc Y. 2008. Numerical Modeling of Bedform Development in Turbulent Flows. Doctoral Dissertation, Ritsumeikan University, Kusatsu, Japan.

Nguyen, Q.Y., and Wells, J.C. 2008. Numerical Modelling of Bedform Development; Formation of Sand-Wavelets in Hydrodynamically Smooth Flow over an Erodible Bed. Annual Journal of Hydraulic Engineering, JSCE. 52: 163-168.

Nguyen, Q.Y., and Wells, J.C. 2009. A Numerical Model to Study Bedform Development in Hydraulically Smooth Turbulent Flows. Annual Journal of Hydraulic Engineering, JSCE. 53: 157-162.

Phillips, B.C., and A.J. Sutherland. 1989. Spatial Lag Effects in Bed Load Sediment Transport. Journal of Hydraulic Research JHYRAF. 27(1).

Raudkivi, A.J. 1997. Ripples on Stream Bed. J. Hydr. Engrg. 123(1): 58-64.

Richards, K.J. 1980. The Formation of Ripples and Dunes on an Erodible Bed. Journal of Fluid Mechanics. 99(03): 597-618.

van Rijn, L.C. 1984. Sediment Transport, Part I: Bed Load Transport. Journal of Hydraulic Engineering. 110(10): 1431–1456.

Sumer, B.M., and M. Bakioglu. 1984. Formation of Ripples on an Erodible Bed. Journal of Fluid Mechanics. 144.

Thuc, T. 1991. Two-dimensional morphological computations near hydraulic structures. Doctoral Dissertation, Asian Institute of Technology, Bangkok, Thailand.

Wu, W., D.A. Vieira, and S.S. Wang. 2004. One-Dimensional Numerical Model for Nonuniform Sediment Transport under Unsteady Flows in Channel Networks. Journal of Hydraulic Engineering. 130(9): 914–923.

Yalin. M. S. 1977. Mechanics of Sediment Transport. 2nd ed. Pergamon Press.

Zedler, E.A., and R.L. Street. 2001. Large-Eddy Simulation of Sediment Transport: Currents over Ripples. J. Hydr. Engrg. 127(6): 444-452.